The Astrophysical Journal, 690:1018–1030, 2009 January 1 doi:10.1088/0004-637X/690/1/1018

MULTIWAVELENGTH OBSERVATIONS OF 3C 454.3. I. THE *AGILE* 2007 NOVEMBER CAMPAIGN ON THE "*CRAZY DIAMOND*"

S. Vercellone[1], A. W. Chen[1,2], V. Vittorini[3], A. Giuliani[1], F. D'Ammando[3,4], M. Tavani[3,4], I. Donnarumma[3], G. Pucella[3], C. M. Raiteri[5], M. Villata[5], W. P. Chen[6], G. Tosti[7], D. Impiombato[7], P. Romano[8], A. Belfiore[9], A. De Luca[1,9,10], G. Novara[11], F. Senziani[1,9], A. Bazzano[3], M. T. Fiocchi[3], P. Ubertini[3], A. Ferrari[2,12], A. Argan[3], G. Barbiellini[6], F. Boffelli[10,11], A. Bulgarelli[13], P. Caraveo[1], P. W. Cattaneo[10], V. Cocco[3], E. Costa[3], E. Del Monte[3], G. De Paris[3], G. Di Cocco[13], Y. Evangelista[3], M. Feroci[3], M. Fiorini[1], F. Fornari[1], T. Froysland[3,14], F. Fuschino[13], M. Galli[15], F. Gianotti[13], C. Labanti[13], I. Lapshov[3], F. Lazzarotto[3], P. Lipari[16], F. Longo[17], M. Marisaldi[13], S. Mereghetti[1], A. Morselli[14], A. Pellizzoni[1], L. Pacciani[3], F. Perotti[1], P. Picozza[14], M. Prest[18], M. Rapisarda[19], A. Rappoldi[10], P. Soffitta[3], M. Trifoglio[13], A. Trois[3], E. Vallazza[6], A. Zambra[1], D. Zanello[16], C. Pittori[20], F. Verrecchia[20], P. Santolamazza[20], B. Preger[20], D. Gasparrini[20], S. Cutini[20], P. Giommi[20], S. Colafrancesco[20], and L. Salotti[21]

[1] Istituto Nazionale di Astrofisica/Istituto di Astrofisica Spaziale e Fisica Cosmica–Milano, Via E. Bassini 15, I-20133 Milano, Italy; stefano@iasf-milano.inaf.it
[2] Consorzio Interuniversitario per la Fisica Spaziale–Torino, Viale Settimio Severo 3, I-10133 Torino, Italy
[3] Istituto Nazionale di Astrofisica/Istituto di Astrofisica Spaziale e Fisica Cosmica–Roma, Via del Fosso del Cavaliere 100, I-00133 Roma, Italy
[4] Dip. di Fisica, Univ. "Tor Vergata", Via della Ricerca Scientifica 1, I-00133 Roma, Italy
[5] Istituto Nazionale di Astrofisica/Osservatorio Astronomico di Torino, Via Osservatorio 20, I-10025 Pino Torinese, Italy
[6] Istitute of Astronomy, National Central University, Taiwan
[7] Dip. di Fisica, Univ. di Perugia, Via Pascoli, I-06123 Perugia, Italy
[8] Consorzio Interuniversitario per la Fisica Spaziale–Palermo, Via U. La Malfa 153, I-90146 Palermo, Italy
[9] Ist. Univ. di Studi Superiori, V. le Lungo Ticino 56, I-27100 Pavia, Italy
[10] Istituto Nazionale di Fisica Nucleare–Pavia, Via Bassi 6, I-27100 Pavia, Italy
[11] Dip. di Fisica Nucleare e Teorica, Univ. degli Studi di Pavia, Via Bassi 6, I-27100 Pavia, Italy
[12] Dip. di Fisica, Univ. di Torino, Via P. Giuria 1, I-10125 Torino, Italy
[13] Istituto Nazionale di Astrofisica/Istituto di Astrofisica Spaziale e Fisica Cosmica–Bologna, Via Gobetti 101, I-40129 Bologna, Italy
[14] Istituto Nazionale di Fisica Nucleare–Roma "Tor Vergata", Via della Ricerca Scientifica 1, I-00133 Roma, Italy
[15] Ente per le Nuovo Tecnologie, l'Energia e l'Ambiente–Bologna, Via Martiri di Monte Sole 4, I-40129 Bologna, Italy
[16] Istituto Nazionale di Fisica Nucleare–Roma "La Sapienza", Piazzale A. Moro 2, I-00185 Roma, Italy
[17] Dip. di Fisica and INFN, Via Valerio 2, I-34127 Trieste, Italy
[18] Dip. di Fisica, Univ. dell'Insubria, Via Valleggio 11, I-22100 Como, Italy
[19] Ente per le Nuovo Tecnologie, l'Energia e l'Ambiente–Roma, Via E. Fermi 45, I-00044 Frascati (Roma), Italy
[20] Agenzia Spaziale Italiana–Science Data Center, Via G. Galilei, I-00044 Frascati (Roma), Italy
[21] Agenzia Spaziale Italiana, Viale Liegi 26, I-00198 Roma, Italy
Received 2008 August 14; accepted 2008 September 9; published 2008 December 1

ABSTRACT

We report on a multiwavelength observation of the blazar 3C 454.3 (which we dubbed *crazy diamond*) carried out on November 2007 by means of the astrophysical satellites *AGILE*, *International Gamma-Ray Astrophysics Laboratory* (*INTEGRAL*), *Swift*, the Whole Earth Blazar Telescope (WEBT) Consortium, and the optical–NIR telescope Rapid Eye Mount (REM). Thanks to the wide field of view of the *AGILE* satellite and its prompt alert dissemination to other observatories, we obtained a long (three weeks), almost continuous γ-ray coverage of the blazar 3C 454.3 across 14 decades of energy. This broadband monitoring allows us to study in great detail light curves, correlations, time lags, and spectral energy distributions (SEDs) during different physical states. Gamma-ray data were collected during an *AGILE* pointing toward the Cygnus Region. Target of Opportunity (ToO) observations were performed to follow up the γ-ray observations in the soft and hard X-ray energy bands. Optical data were acquired continuously by means of a preplanned WEBT campaign and through an REM ToO repointing. 3C 454.3 is detected at a $\sim 19\sigma$ level during the three-week observing period, with an average flux above 100 MeV of $F_{E>100\,\mathrm{MeV}} = (170 \pm 13) \times 10^{-8}$ photons cm^{-2} s^{-1}. The γ-ray spectrum can be fitted with a single power law with photon index $\Gamma_{\mathrm{GRID}} = 1.73 \pm 0.16$ between 100 MeV and 1 GeV. We detect significant day-by-day variability of the γ-ray emission during our observations, and we can exclude that the fluxes are constant at the 99.6% ($\sim 2.9\sigma$) level. The source was detected typically around 40 deg off-axis, and it was substantially off–axis in the field of view of the *AGILE* hard X-ray imager. However, a five-day long ToO observation by *INTEGRAL* detected 3C 454.3 at an average flux of about $F_{20\text{–}200\,\mathrm{keV}} = 1.49 \times 10^{-3}$ photons cm^{-2} s^{-1}with an average photon index of $\Gamma_{\mathrm{IBIS}} = 1.75 \pm 0.24$ between 20–200 keV. *Swift* also detected 3C 454.3 with a flux in the 0.3–10 keV energy band in the range (1.23–1.40) $\times 10^{-2}$ photons cm^{-2} s^{-1} and a photon index in the range $\Gamma_{\mathrm{XRT}} = 1.56$–$1.73$. In the optical band, both WEBT and REM show an extremely variable behavior in the *R* band. A correlation analysis based on the entire data set is consistent with no time lags between the γ-ray and the optical flux variations. Our simultaneous multifrequency observations strongly indicate that the dominant emission mechanism between 30 MeV and 30 GeV is dominated by inverse Compton scattering of relativistic electrons in the jet on the external photons from the broad line region.

Key words: galaxies: active – galaxies: jets – quasars: general – quasars: individual (3C 454.3) – radiation mechanisms: non-thermal

Online-only material: color figures

1. INTRODUCTION

Among active galactic nuclei (AGNs), blazars show intense and variable γ-ray emission above 100 MeV (Hartman et al. 1999). Variability timescale can be as short as a few days, or last a few weeks. They emit across several decades of energy, from the radio to the TeV energy band. Blazar spectral energy distributions (SEDs) are typically double-humped, with a first peak occurring in the IR/optical band in the so-called *red blazars* (including Flat Spectrum Radio Quasars (FSRQs), and low-energy-peaked BL Lacs (LBLs)) and at UV/X-rays in the so-called *blue blazars* (including high-energy-peaked BL Lacs (HBLs)), and it is commonly interpreted as synchrotron radiation from high-energy electrons in a relativistic jet. The second SED component, which peaks at MeV–GeV energies in red blazars and at TeV energies in blue blazars, is commonly interpreted as inverse Compton (IC) scattering of soft seed photons by relativistic electrons. A recent review of the blazar emission mechanisms and energetics is given in Celotti & Ghisellini (2008). Alternatively, the blazar SED can be explained in the framework of the hadronic models, where the relativistic protons in the jet are the primary accelerated particles, emitting γ-ray radiation by means of photo-pair and photo-pion production (see Mücke & Protheroe 2001; Mücke et al. 2003 for a recent review on hadronic models).

Multiwavelength studies of variable γ-ray blazars have been carried out since the beginning of the 1990s, thanks to the *Compton Gamma Ray Observatory* (*CGRO*). Nevertheless, only a few objects were detected on a timescale of about two weeks in the γ-ray energy band, and simultaneously monitored at different energies, obtaining a multifrequency coverage. Among the FSRQs detected at energies above 100 MeV by the EGRET telescope onboard the *CGRO* (Hartman et al. 1999), 3C 454.3 (PKS 2251+158; $z = 0.859$) is certainly one of the most active at high energy. In the EGRET era, it was detected in 1992 during an intense γ-ray flaring episode (Hartman et al. 1992; 1993) when its flux $F_{E>100\,\mathrm{MeV}}$ was observed to vary within the range $(0.4–1.4) \times 10^{-6}$ photons cm^{-2} s^{-1}. In 1995, a two-week campaign detected a γ-ray flux $< 1/5$ of its historical maximum (Aller et al. 1997).

In 2005, 3C 454.3 underwent a major flaring activity in almost all energy bands (see Giommi et al. 2006). In the optical, it reached $R = 12.0$ mag (Villata et al. 2006) and it was detected by *International Gamma-Ray Astrophysics Laboratory* (*INTEGRAL*) at a flux[22] level of $\sim 3 \times 10^{-2}$ photons cm^{-2} s^{-1} in the 3–200 keV energy band (Pian et al. 2006). Since the detection of the exceptional 2005 outburst, several monitoring campaigns were carried out to follow the source multifrequency behavior (Villata et al. 2006, 2007; Raiteri et al. 2007, 2008a, 2008b). During the last of these campaigns, 3C 454.3 underwent a new optical brightening in mid-July 2007, which triggered observations at all frequencies.

In 2007 July, Vercellone et al. (2008, hereafter V08) reported the highest γ-ray flare from 3C 454.3. During the period 2007 July 24–30, the average γ-ray flux was $F_{E>100\,\mathrm{MeV}} = (280 \pm 40) \times 10^{-8}$ photons cm^{-2} s^{-1}, about a factor of 2 higher than in 1995. No emission was detected by *Super-AGILE* in the energy range 20–60 keV, with a 3σ upper limit of 2.3×10^{-3} photons cm^{-2} s^{-1}.

By means of *AGILE* preliminary flux estimate (Vercellone et al. 2007), Ghisellini et al. (2007) compared the 3C 454.3 SEDs obtained during three multiwavelength campaigns (2000, 2005, and 2007). The 2007 data show that the γ-ray high state occurred during a weaker optical/X-ray flux compared with the 2005 flare.

In this paper (Paper I), we present the results of a multiwavelength campaign on 3C 454.3 during a long-lasting γ-ray activity period between 2007 November 10 and December 1. Preliminary γ-ray results were distributed in Chen et al. (2007), while radio-to-optical and UV data were published in Raiteri et al. (2008a). A companion paper (Paper II, I. Donnarumma et al. 2008, in preparation) will describe the *AGILE* multiwavelength campaign during December 2007. In Section 2, we present the multiwavelength campaign on 3C 454.3; in Sections 3 through 6 we present the *AGILE*/GRID (Gamma-Ray Imaging Detector), *INTEGRAL*/IBIS, *Swift*/XRT (X-ray Telescope), Whole Earth Blazar Telescope (WEBT), and Rapid Eye Mount (REM) data analysis, respectively; in Section 7, we present the simultaneous multiwavelength light curves and SEDs. In Sections 8 and 9, we discuss our results and draw our conclusions. Throughout this paper the quoted uncertainties are given at the 1σ level, unless otherwise stated.

2. THE MULTIWAVELENGTH CAMPAIGN

In 2007 November, *AGILE* began pointing 3C 454.3 at high off-axis angle (about 40°). Nevertheless, in a few days 3C 454.3 was detected at more than 5σ (Chen et al. 2007), exhibiting variable activity on a day timescale (Pucella et al. 2007). Immediately after the source detection, a multiwavelength campaign started. *AGILE* data were collected during two different periods, the first ranging between 2007 November 10 12:17 UT and 2007 November 25 10:57 UT and the second between 2007 November 28 12:05 UT and 2007 December 1 11:39 UT, for a total of about 592 ks. The three-day gap between them was due to a preplanned GRID calibration activity. *INTEGRAL* data were collected during a dedicated Target of Opportunity (ToO) on revolutions 623 (between 2007 November 20 03:35 UT and 2007 November 22 08:46 UT) and 624 (between 2007 November 22 20:45 UT and 2007 November 24 15:50 UT), for a total of about 300 ks, while *Swift*/XRT data were obtained during several ToO pointings for a total of about 10 ks. WEBT data (radio-to-optical) as well as *Swift*/UVOT data were published in Raiteri et al. (2008a), while REM data were acquired following a ToO request. In both cases, optical data were acquired continuously during the whole *AGILE* campaign.

3. *AGILE* DATA

3.1. Data Reduction and Analysis

The *AGILE* satellite (Tavani et al. 2008a, 2008b), a mission of the Italian Space Agency (ASI) devoted to high-energy astrophysics, is currently the only space mission capable of observing cosmic sources simultaneously in the energy bands 18–60 keV and 30 MeV–50 GeV. The satellite was launched on 2007 April 23 by the Indian PSLV-C8 rocket from the Satish Dhawan Space Center SHAR, Sriharikota.

The *AGILE* scientific instrument is very compact and combines four active detectors yielding broadband coverage from hard X-rays to γ-rays: a silicon tracker (ST; Prest et al. 2003, 30 MeV–50 GeV), a co-aligned coded-mask hard X-ray imager (SA; Feroci et al. 2007, 18–60 keV), a non-imaging CsI mini-calorimeter (MCAL; Labanti et al. 2006, 0.3–100 MeV), and a segmented anti-coincidence system (ACS;

[22] Assuming a Crab-like spectrum.

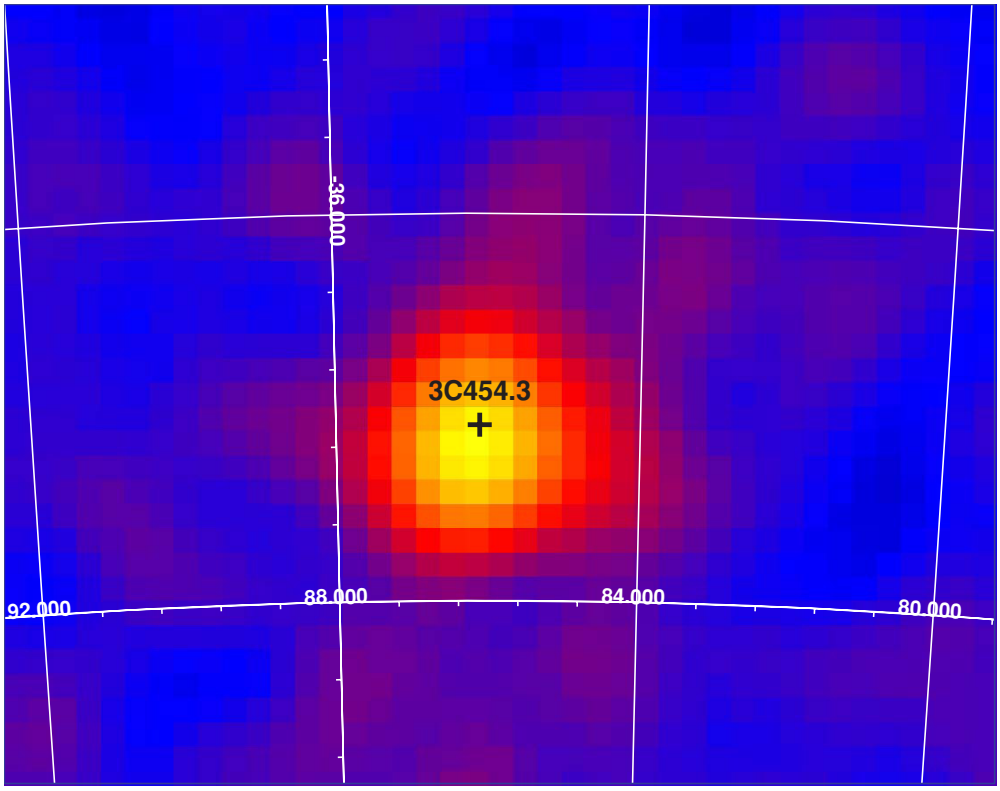

Figure 1. Gaussian-smoothed intensity map (∼10° × 08°) in Galactic coordinates integrated over the whole observing period (2007 November 10 12:17 UT–2007 December 01 11:39 UT). The cross symbol is located at the 3C 454.3 radio coordinates.

(A color version of this figure is available in the online journal.)

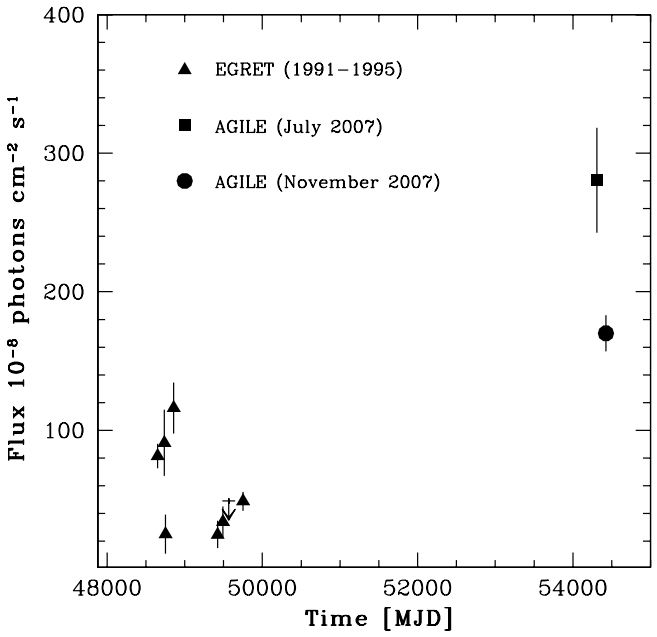

Figure 2. EGRET (triangles) and *AGILE* GRID (square and circle) γ-ray light curve in units of 10^{-8} photons cm^{-2} s^{-1}. EGRET data are from Hartman et al. (1999). *AGILE* July 2007 data are from V08.

Perotti et al. 2006). Gamma-ray detection is obtained by the combination of ST, MCAL, and ACS; these three detectors form the *AGILE* GRID.

Level 1 *AGILE* GRID data were analyzed using the *AGILE* Standard Analysis Pipeline (see V08 for a detailed discussion of the *AGILE* data reduction). Since 3C 454.3 was at a high off-axis angle, an ad hoc γ-ray analysis was performed. We used γ-ray events filtered by means of the `FT3ab_2` *AGILE* Filter Pipeline. Counts, exposure, and Galactic background γ-ray maps are created with a bin size of 0.°25 × 0.°25, for $E \geqslant 100$ MeV. Since the source was at 40° off-axis, all the maps were generated including all events collected up to 60 deg off-axis. We rejected all the γ-ray events whose reconstructed directions form angles with the satellite–Earth vector smaller than 80° (`albrad=80`), reducing the γ-ray Earth albedo contamination by excluding regions within ∼ 10° from the Earth limb. The most recent versions (`BUILD-15`) of the calibration files, which will be publicly available at the ASI Science Data Centre (ASDC[23]) site, and of the γ-ray diffuse emission model (Giuliani et al. 2004) were used. The first step consists in running the *AGILE* Source Location task in order to derive the most plausible location of the source. In the second step, we ran the *AGILE* maximum likelihood analysis (`ALIKE`) using a radius of analysis of 10°, and the best-guess position derived in the first step. The particular choice of the radius of analysis parameter is dictated to avoid any possible contamination by very off-axis residual particle events.

3.2. Results

Figure 1 shows a Gaussian-smoothed intensity map (∼10° × 08°) in Galactic coordinates integrated over the whole observing period, using the selections described in Section 3.1. The source detection significance is 19σ and the average γ-ray flux above 100 MeV for the whole period is $F_{E>100\,\mathrm{MeV}} = (170 \pm 13) \times 10^{-8}$ photons cm^{-2} s^{-1}, as derived from the *AGILE* maximum likelihood code analysis. We note that the average γ-ray flux computed over the three-week campaign is lower than

[23] http://agile.asdc.asi.it.

$F^{\rm July}_{E>100\,{\rm MeV}} = (280 \pm 40) \times 10^{-8}$ photons cm^{-2} s^{-1}, observed during the flaring episode in July 2007, and computed during only a six-day observation. Nevertheless, Figure 2 shows that the current average flux is still higher than those observed during the EGRET era. The smaller errors on the *AGILE* November data with respect to the July data are due to both the higher statistics (323 versus 101 counts collected in November and in July, respectively), and the more accurate calibration response files.

Figure 3 shows the γ-ray light curve at one-day resolution for photons above 100 MeV. We note that 3C 454.3 is detected at a 3σ level during almost the whole period on a one-day timescale; this clearly indicates strong γ-ray flaring activity.

The average γ-ray flux as well as the daily values of the 18 days were derived according to the γ-ray analysis procedure described in Mattox et al. (1993). First, the entire period was analyzed to determine the diffuse gas parameters and then the source flux density was estimated independently for each of the 18 one-day periods, with the diffuse parameters fixed at the values obtained in the first step. Fitting the GRID fluxes to a constant model (the weighted mean of the one-day average flux values) yields $F_{\rm wtd} = (186.3 \pm 14.6) \times 10^{-8}$ photons cm^{-2} s^{-1}. Following McLaughlin et al. (1996), we computed the variability coefficient V. The 2σ upper limits (UL) were properly treated, assigning a value and a sigma equal to UL/2 (Torres et al. 2001). We obtain a $\chi^2 = 36.7$ for 17 degrees of freedom (dof); therefore we can exclude that the fluxes are constant at the 99.6% ($\sim 2.9\sigma$) level, and we obtain a value for the variability coefficient V of 2.43. A value of $V > 1$ indicates that the source is variable within the observed period.

Figure 4 shows the average γ-ray spectrum derived over the entire observing period. The average spectrum was obtained by computing the γ-ray flux in five energy bins over the entire observing period: $50 < E < 100$ MeV, $100 < E < 200$ MeV, $200 < E < 400$ MeV, $400 < E < 1000$ MeV, and $1000 < E < 3000$ MeV. We fit the data by means of a simple power-law model and restricted our fit to the most reliable energy range (100 MeV–1 GeV):

$$F(E) = 3.61 \times 10^{-5} \left(\frac{E}{1\,{\rm MeV}}\right)^{-(1.73\pm0.16)} \text{photons cm}^{-2}\ \text{s}^{-1}\ \text{MeV}^{-1}. \quad (1)$$

Unfortunately, the source was located substantially off-axis in the *Super-AGILE* field of view (FOV) during the whole observation period, resulting in a not particularly constraining upper limit flux, being as high as 1.13×10^{-2} photons cm^{-2} s^{-1} (50 mCrab).

4. *INTEGRAL* DATA

4.1. Data Reduction and Analysis

The ESA *INTEGRAL* γ-ray Observatory, launched in 2002 October, carries three co-aligned coded-mask telescopes. For the purpose of this paper, we refer to data from the IBIS instrument (Ubertini et al. 2003), sensitive in the energy range 15 keV–10 MeV and with an FoV of $29^\circ \times 29^\circ$, and in particular to the ISGRI lower energy detector layer.

All the observations are organized into uninterrupted 2000–3600 s long science windows (SCW): light curves and spectra were extracted for each individual SCW. Wide-band spectra (from 17 to 150 keV) of the source were obtained using data from the IBIS instrument. All the data were processed using the Off-line Scientific Analysis (OSA) version 7.0 software released by the *INTEGRAL* Scientific Data Centre. *INTEGRAL* data were analyzed using FTOOLS and XSPEC11.3.2 in the `Heasoft` package (ver. 6.4). We assumed a single power-law model to fit the IBIS data.

Table 1
INTEGRAL/IBIS Spectral Fit Results

Rev.	Γ	$\chi^2_{\rm red}$ (dof)	Flux[a]
623	$1.78^{+0.33}_{-0.30}$	1.21 (11)	1.52
624	$1.71^{+0.41}_{-0.36}$	0.54 (11)	1.42
623+624	$1.75^{+0.25}_{-0.23}$	0.89 (11)	1.49

Note. [a] Flux in the 20–200 keV band in units of 10^{-3} photons cm^{-2}s^{-1} obtained from the spectral fits.

Figure 5 shows the *INTEGRAL*/IBIS light curve in the energy range 20–50 keV accumulated during the whole observation. The source does not show statistically significant flux variations. Figure 6 shows the *INTEGRAL*/IBIS spectra for revolution 623 (red circles), revolution 624 (blue triangles), and for the whole observation (black squares).

Table 1 summarizes the *INTEGRAL*/IBIS spectral fit results.

5. *Swift* DATA

5.1. Data Reduction and Analysis

The NASA *Swift* γ-ray Burst Mission (Gehrels et al. 2004), launched in 2004 November, has three co-aligned instruments: a coded-mask Burst Alert Telescope (BAT; Barthelmy et al. 2005, 15–150 keV), an X-ray Telescope (XRT; Burrows et al. 2005, 0.2–10 keV), and an Ultraviolet/Optical Telescope (UVOT; Roming et al. 2005, 170–600 nm).

Swift data (Obs. ID 00031018) were collected by activating a *Swift* Cycle-3 Proposal (PI: A. W. Chen) and by means of a dedicated ToO triggered by *AGILE* (PI: S. Vercellone). The XRT data were processed with standard procedures (`xrtpipeline` v0.11.6), adopting the standard filtering and screening criteria, and using FTOOLS in the `Heasoft` package (ver. 6.4). The source count rate was low during the whole campaign; thus we only considered photon counting data (PC) and further selected XRT event grades 0–12 (Burrows et al. 2005). *Swift*/XRT data show an average count rate of > 0.5 counts s^{-1}, and therefore a pile-up correction was required. We extracted the source events from an annular source extraction region with an inner radius of 2–3 pixels (estimated case-by-case by means of the point-spread function (PSF) fitting technique) and an outer radius of 30 pixels (1 pixel $\sim$ 2.″37). To account for the background, we also extracted events within a circular region centered on a region free from background sources and with radius of 80 pixels. Ancillary response files were generated with `xrtmkarf`, and account for different extraction regions, vignetting, and PSF corrections. We used the spectral redistribution matrices v010 in the Calibration Database maintained by HEASARC. *Swift*/XRT uncertainties are given at 90% confidence level for one interesting parameter (i.e., $\Delta\chi^2 = 2.71$) unless otherwise stated.

Figure 7 shows the 0.3–10 keV spectra for segments 001–006, where we summed segments 003 and 004 in order to have similar statistics as the others: black circles (segm. 001), red squares (segm. 003+004), green upside-down triangles (segm. 005), and cyan stars (segm. 006). Segment 002 was not considered, since only 1 s of data were recorded. We

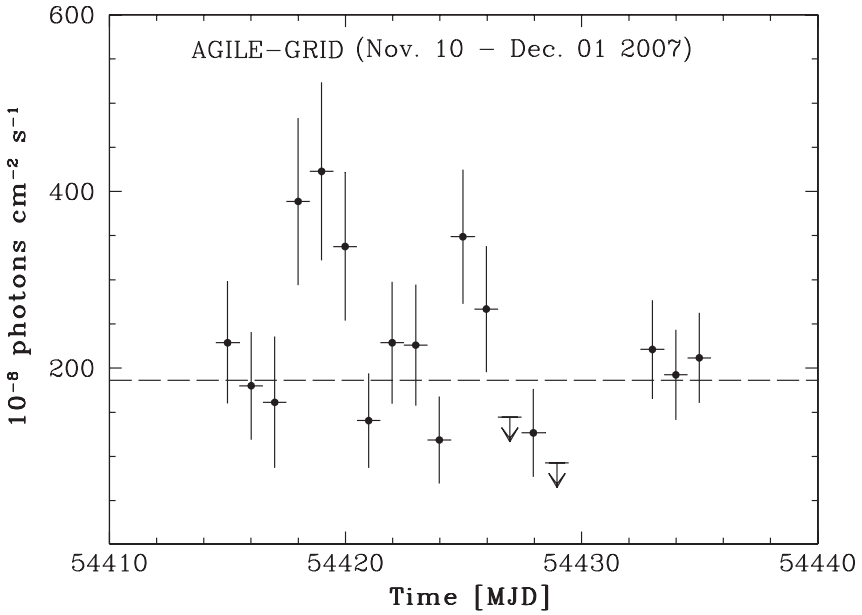

Figure 3. *AGILE* GRID γ-ray light curve at $\approx$ one-day resolution for $E > 100$ MeV in units of 10^{-8} photons cm^{-2} s^{-1}. The downward arrows represent 2σ upper limits. The dashed line represents the weighted mean flux.

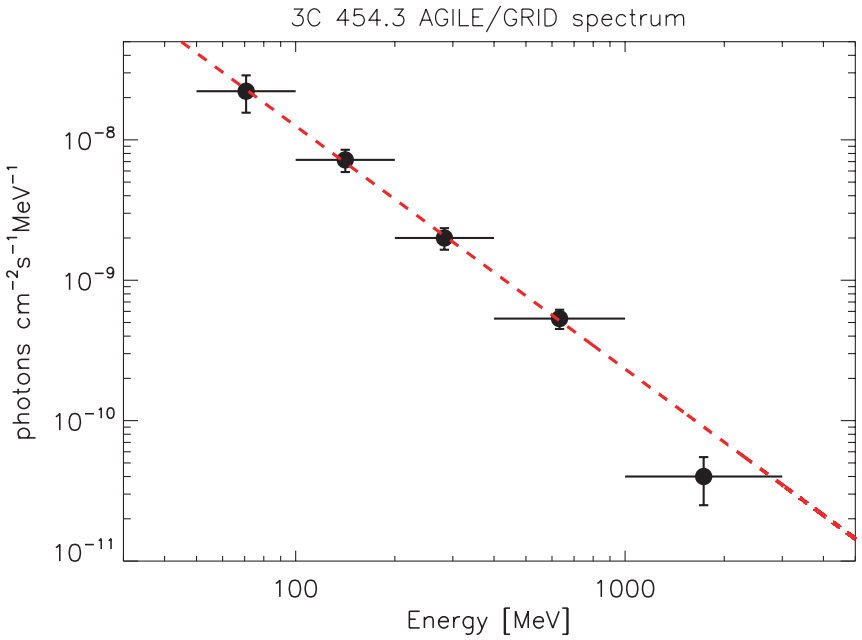

Figure 4. *AGILE* GRID average γ-ray spectrum. Three energy bins were considered: $100 < E < 200$ MeV, $200 < E < 400$ MeV, $400 < E < 1000$ MeV. The red dashed line represents the best-fit power-law model.

(A color version of this figure is available in the online journal.)

first fit *Swift*/XRT spectra with an absorbed power-law model, named model A (`wabs*zwabs(powerlaw)` in `XSPEC 11.3.2`). Data were rebinned in order to have at least 20 counts per energy bin. The Galactic absorption was fixed to the value of $N_{\rm H}^{\rm Gal} = 0.724 \times 10^{21}$ cm^{-2} (Kalberla et al. 2005). We considered, in addition to the Galactic absorption coefficient, an extra absorption component, $N_{\rm H}^{z}$, following the results shown in Ghisellini et al. (2007) and Raiteri et al. (2007). A second spectral fit (model B) was performed considering a simple power law, with the absorption component as a free parameter (`wabs*(powerlaw)`). Table 2 summarizes the most relevant spectral fit parameters.

We note that the $N_{\rm H}^{z}$ component in model A is not well constrained, while a simpler fit (model B) characterized by a single power-law model with free absorption coefficient yields $N_{\rm H}$ values which are consistent within the uncertainties among different observations. We also check the possible presence of a double power law as reported in Raiteri et al. (2008b) as follows. We fixed the $N_{\rm H}$ to the value derived by Villata et al. (2006), $(1.34 \pm 0.05) \times 10^{21}$ cm^{-2} (based on *Chandra* data), and fixed the hard power-law index to the one we obtained by fitting the XRT data above 2 keV. In most cases, the harder power-law component is not required, as its normalization is consistent with zero.

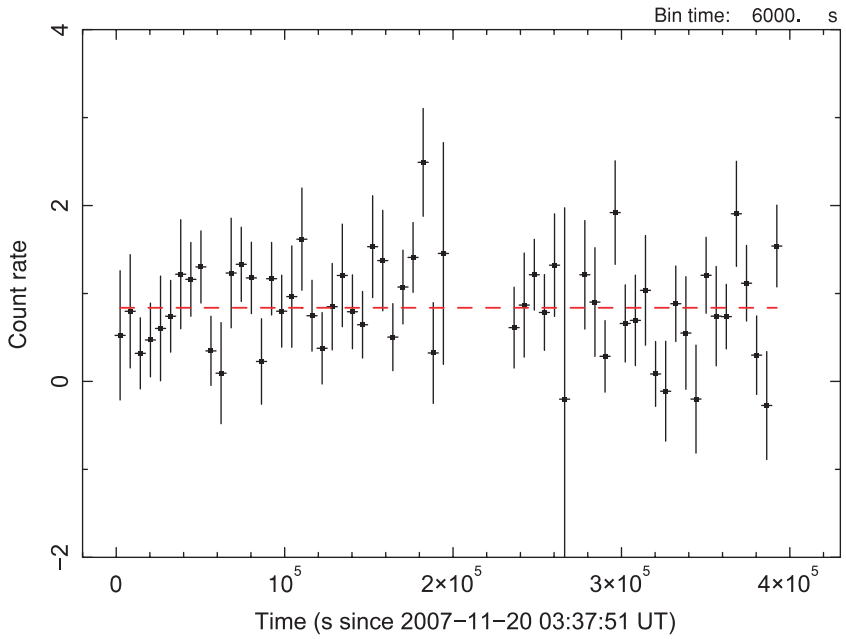

Figure 5. *INTEGRAL*/IBIS light curve in the energy range 20–50 keV accumulated during the whole observation. The dashed line represents a fit with a constant model.

(A color version of this figure is available in the online journal.)

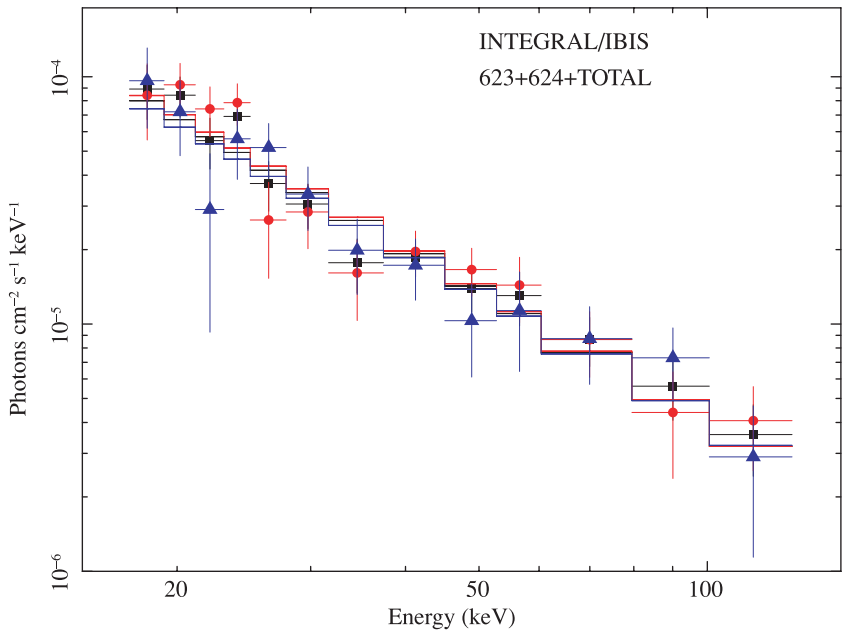

Figure 6. *INTEGRAL*/IBIS spectra for revolution 623 (red circles), revolution 624 (blue triangles), and for the whole observation (black squares).

(A color version of this figure is available in the online journal.)

Figure 8 shows the *Swift*/XRT photon index versus the 0.3–10 keV flux. Numbers beneath each point represent the observing segment.

We analyzed *Swift*/BAT survey data in order to study the hard X-ray emission of 3C 454.3 and to investigate its evolution as a function of time. We selected two time windows, the first between 2005 April 01 and 2005 September 30 (when intense activity was recorded from the target; see, e.g., Giommi et al. (2006)), and the second between 2007 June 01 and 2007 December 31. We considered all BAT observations with 3C 454.3 in the FOV. After a careful data selection, based on background rate, pointing stability, and several other data quality criteria (see Senziani et al. 2007), we ended up with 4824 observations for a net exposure time of $\sim$ 792 ks in six months in 2005 and $\sim$ 624 ks in seven months in 2007.

Here we provide a brief overview of the BAT survey data analysis procedure, while a detailed description will be addressed in a forthcoming paper (A. Belfiore et al. 2008, in preparation). Starting from detector plane histogram (DPH) files, detector plane images (DPI) in the 20–60 keV and 60–100 keV energy range were generated and were cleaned from hot pixels and noisy detectors. Then, with the HEASOFT task *batfftimage* each DPI was deconvolved to obtain a background- and source-subtracted sky image of the BAT FOV. For each

Table 2
Swift/XRT Spectral Fit Results

Obs.[a]	$N_{\rm H}$ (10^{22} cm^2)	Γ	$\chi^2_{\rm red}$/(dof)	$F_{0.3{\rm badhbox10}}$ (obs.) (photons cm^{-2} s^{-1})	$F_{2{\rm badhbox10}}$ (obs.) (photons cm^{-2} s^{-1})
Model A: Single Power Law with Galactic+Intrinsic Absorption					
001	$0.0724+(0.06^{+0.06}_{-0.06})$	$1.56^{+0.07}_{-0.07}$	1.173/(108)	1.45×10^{-2}	0.52×10^{-2}
003+004	$0.0724+(0.20^{+0.11}_{-0.10})$	$1.68^{+0.11}_{-0.10}$	0.933/(53)	1.41×10^{-2}	0.51×10^{-2}
005	$0.0724+(0.23^{+0.14}_{-0.12})$	$1.60^{+0.12}_{-0.12}$	0.900/(46)	1.43×10^{-2}	0.56×10^{-2}
006	$0.0724+(0.25^{+0.88}_{-0.78})$	$1.68^{+0.09}_{-0.09}$	1.089/(80)	1.28×10^{-2}	0.48×10^{-2}
Model B: Single Power Law with Free Absorption					
001	$0.10^{+0.02}_{-0.02}$	$1.56^{+0.07}_{-0.07}$	1.100/(131)	1.39×10^{-2}	0.51×10^{-2}
003+004	$0.15^{+0.04}_{-0.03}$	$1.73^{+0.13}_{-0.12}$	0.921/(53)	1.40×10^{-2}	0.50×10^{-2}
005	$0.15^{+0.04}_{-0.03}$	$1.66^{+0.12}_{-0.11}$	1.070/(58)	1.35×10^{-2}	0.52×10^{-2}
006	$0.16^{+0.03}_{-0.02}$	$1.72^{+0.09}_{-0.09}$	1.124/(94)	1.23×10^{-2}	0.46×10^{-2}

Note. [a] Last three digits of observation number 00031018.

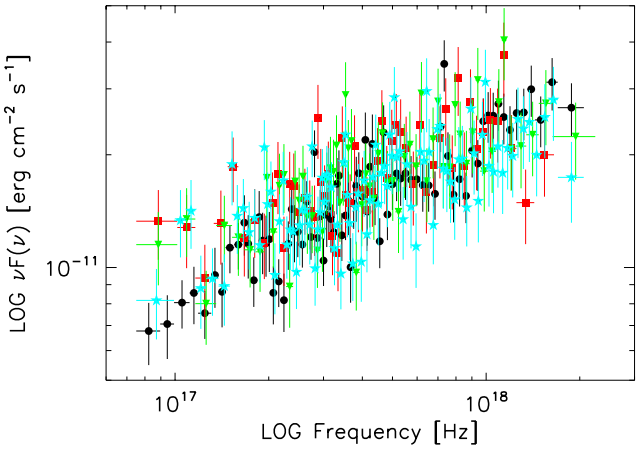

Figure 7. *Swift*/XRT 0.3–10 keV spectra for segments 001 to 006: black circles (segm. 001), red squares (segm. 003+004), green upside-down triangles (segm. 005), and cyan stars (segm. 006).

(A color version of this figure is available in the online journal.)

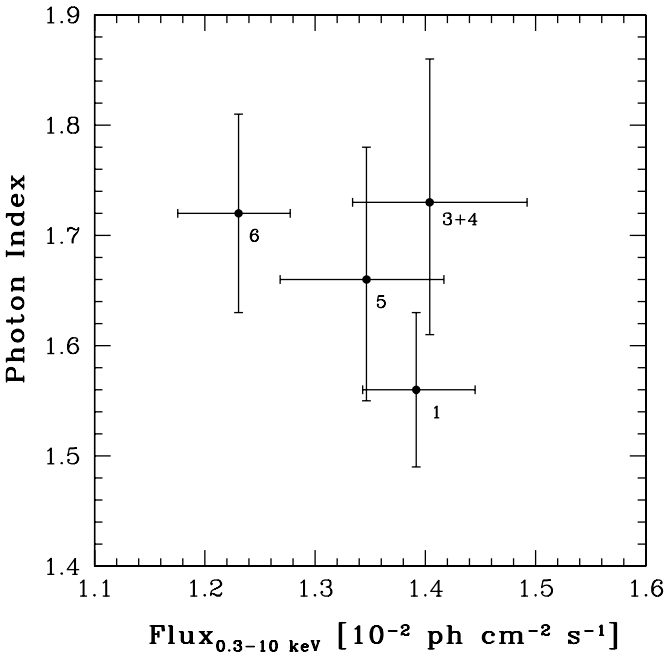

Figure 8. *Swift*/XRT photon index vs. the 0.3–10 keV flux. Numbers beneath each point represent the observing segment. Segment number 2 is missing, since only 1 s of data were recorded.

sky image, an appropriate effective exposure map (weighted on the coded fraction) was generated, accounting for possible Earth/Moon occultations. Then such sky images were reprojected and stacked (weighting on effective exposure) to obtain monthly count rate maps, considering a small portion of the field around the target (a $3^\circ \times 3^\circ$ region in local tangential projection coordinates, TAN).

The count rates of 3C 454.3 were normalized to the Crab count rates and then converted to flux (photons cm^{-2} s^{-1}) assuming for the Crab the canonical power-law spectrum (photon index $\Gamma = 2.15$ and normalization of 10.4 photons cm^{-2} s^{-1} keV^{-1} at 1 keV), and for 3C 454.3 a power-law spectrum with $\Gamma = 1.7$, averaging the instrument response over the FOV. The 2007 November net exposure time is $\sim$ 106 ks for a flux in the 20–60 keV energy band of $(1.07 \pm 0.19) \times 10^{-3}$ photons cm^{-2} s^{-1}.

Figure 9 shows the long-term *Swift*/BAT light curves in the 20–60 keV (bottom panel) and 60–100 keV (upper panel) energy range. The yellow vertical area marks the *AGILE* November campaign. The *Swift*/BAT flux is in good agreement with the flux derived from the whole *INTEGRAL*/IBIS campaign in the same energy range, $F^{\rm IBIS}_{20-60\,{\rm keV}} = 1.02 \times 10^{-3}$ photons cm^{-2} s^{-1}. The short dashed line marks the epoch of the giant optical flare in 2005 (Fuhrmann et al. 2006; Villata et al. 2006), when the hard X-ray flux was about twice higher than in November 2007.

6. OPTICAL DATA

6.1. WEBT Data Reduction and Analysis

The WEBT[24] has been monitoring 3C 454.3 since the exceptional 2004–2005 outburst (Villata et al. 2006, 2007; Raiteri et al. 2007, 2008a, 2008b), covering also the period of the *AGILE* observation. We refer to Raiteri et al. (2008a) for a detailed presentation and discussion of the radio, mm, near-IR, optical and *Swift*/UVOT data collected, almost continuously, during 2007 November.

6.2. REM Data Reduction and Analysis

The photometric optical and near-infrared (NIR) observations were carried out with REM (Zerbi et al. 2004), a robotic telescope located at the ESO Cerro La Silla observatory (Chile). The REM telescope has a Ritchey–Chretien configuration with

[24] http://www.oato.inaf.it/blazar/webt; see e.g. Villata et al. (2004).

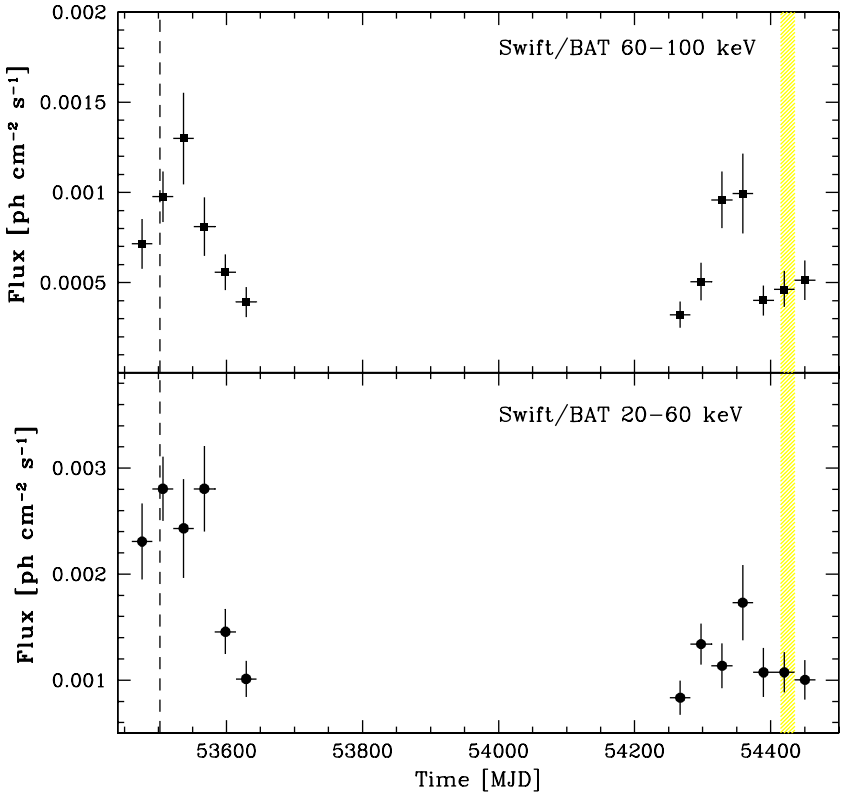

Figure 9. Long-term *Swift*/BAT light curves in the 20–60 keV (bottom panel) and 60–100 keV (upper panel) energy range. The yellow vertical area marks the *AGILE* November campaign. The short dashed line marks the epoch of the giant optical flare in 2005.

(A color version of this figure is available in the online journal.)

a 60 cm f/2.2 primary and an overall f/8 focal ratio in a fast-moving alt-azimuth mount, providing two stable Nasmyth focal stations. At one of the two foci, the telescope simultaneously feeds, by means of a dichroic, two cameras: REMIR for the NIR (Conconi et al. 2004), and ROSS (Tosti et al. 2004) for the optical. Both the cameras have a FOV of $10' \times 10'$ and imaging capabilities with the usual NIR (z', J, H, and K), and Johnson–Cousins V, R, and I filters. All raw optical/NIR frames obtained with REM telescopes were corrected for dark, bias, and flat field. Instrumental magnitudes were obtained via aperture photometry using *Global Astrometric Interferometer for Astrophysics* (GAIA)[25]. Calibration of the optical source magnitude was obtained by differential photometry with respect to the comparison stars sequence reported by Fiorucci et al. (1998) and Raiteri et al. (1998). For the NIR calibration, we used the comparison sequence reported by González-Pérez et al. (2001). Both REMIR and ROSS instruments were used in order to obtain nearly simultaneous data and to study the spectral behavior of 3C 454.3 at different levels of flux.

7. SIMULTANEOUS DATA ANALYSIS

Figure 10 shows the simultaneous light curves acquired during the period 2007 November 6–December 3. Black circles represent *AGILE* GRID data (30 MeV–50 GeV); red triangles represent *INTEGRAL*/IBIS data (20–200 keV); blue pentagons represent *Swift*/XRT data (0.3–10 keV); cyan (solid) and green (open) squares represent R-band WEBT and REM (Raiteri et al. 2008a) data, respectively. The yellow areas mark the periods P1 and P2 during which we compute the simultaneous SEDs, corresponding to higher γ-ray flux levels. We note that during the period P1 the optical flux shows intense variability, reaching a relative maximum on the last day of the γ-ray day-by-day sampling. Moreover, an optical flare as intense as the one on MJD $\sim$ 54,420 occurred at the end of the *AGILE* observations (MJD $\sim$ 54,435.5). The three γ-ray data points show no particular flaring activity, though the daily flux remained quite high, $\sim 200 \times 10^{-8}$ photons cm^{-2} s^{-1}. A detailed discussion on the correlation between the optical and the γ-ray data during December 2007 will be presented in the forthcoming Paper II (I. Donnarumma et al. 2008, in preparation).

We investigated the expected γ–optical flux correlation by means of the discrete correlation function (DCF; see Edelson & Krolik 1988; Hufnagel & Bregman 1992; Peterson 2001). The result is shown in Figure 11. The DCF peak occurred at $\tau = 0$, and its value is $\sim$ 0.5. This indicates a moderate correlation, with no significant time delay between the γ-ray and optical flux variations. A minor peak at $\tau = -5$ days comes from establishing a connection between the optical flare at MJD $\sim$ 54,420 and the high γ flux at MJD $\sim$ 54,425.

Figure 12 shows the SED for the period P1, MJD 54,417.5–54,420.5 (see Figure 10). Filled squares represent the *AGILE* GRID data in the energy range 100–1000 MeV; small filled circles represent *Swift*/XRT data in the energy range 0.3–10 keV (segm. 001); open symbols represent radio-to-UV data taken from Raiteri et al. (2008a), corresponding to MJD 54,420, when all the WEBT UBVRI bands were available, as well as *Swift*/UVOT data.

Figure 13 shows the SED for the period P2, MJD 54,423.5–54,426.5 (see Figure 10). Filled squares represent the *AGILE*

[25] http://star-www.dur.ac.uk/∼pdraper/gaia/gaia.html.

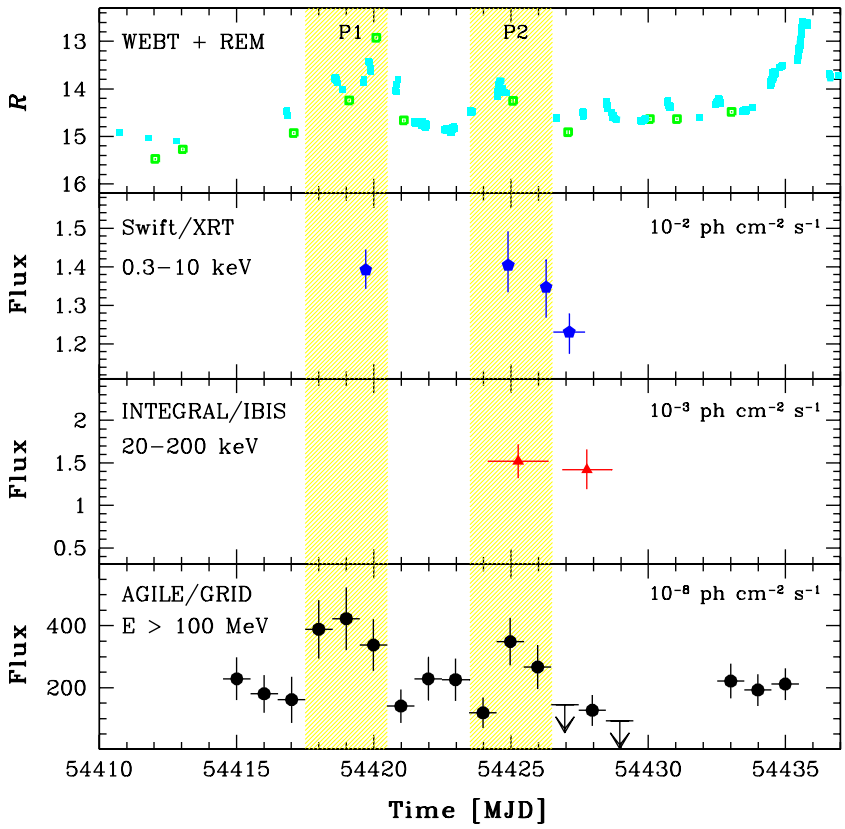

Figure 10. Simultaneous light curves acquired during the period 2007 November 6–December 3. Black circles represent *AGILE* GRID data (30 MeV–50 GeV); red triangles represent *INTEGRAL*/IBIS data (20–200 keV); blue pentagons represent *Swift*/XRT data (0.3–10 keV); cyan (solid) and green (open) squares represent *R*-band WEBT and REM (Raiteri et al. 2008a) data, respectively. The yellow areas mark the periods P1 and P2 during which we compute the simultaneous SEDs.
(A color version of this figure is available in the online journal.)

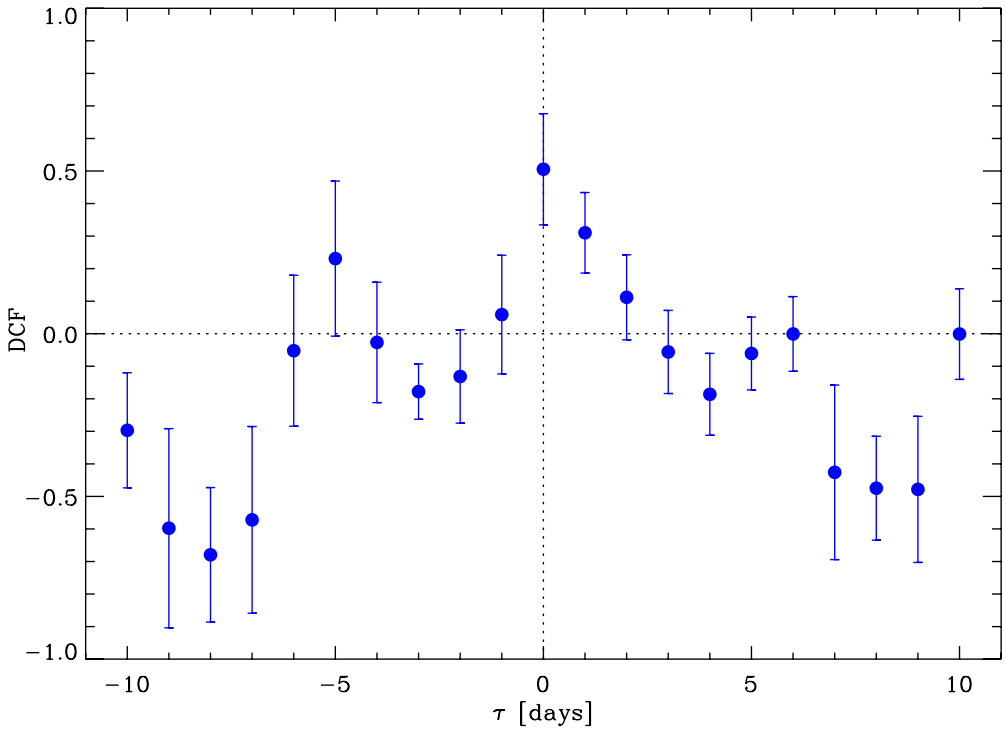

Figure 11. Discrete correlation function between the γ-ray and optical fluxes. The optical data have previously been binned over 12 h to smooth the intranight variations. The DCF peak suggests a mild correlation with no time delay.
(A color version of this figure is available in the online journal.)

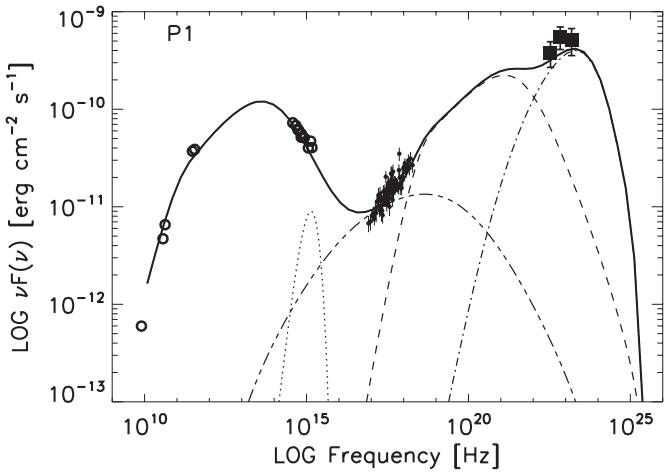

Figure 12. SEDs for the period P1, MJD 54,417.5–54,420.5 (see Figure 10). Filled squares represent the *AGILE* GRID data in the energy range 100–1000 MeV; small filled circles represent *Swift*/XRT data in the energy range 0.3–10 keV (segment 001); open symbols represent radio-to-UV data taken from Raiteri et al. (2008a), corresponding to MJD 54,420. The dotted, dashed, dot–dashed, and triple-dot–dashed lines represent the accretion disk blackbody, the external Compton on the disk radiation, the external Compton on the BLR, and SSC radiation, respectively.

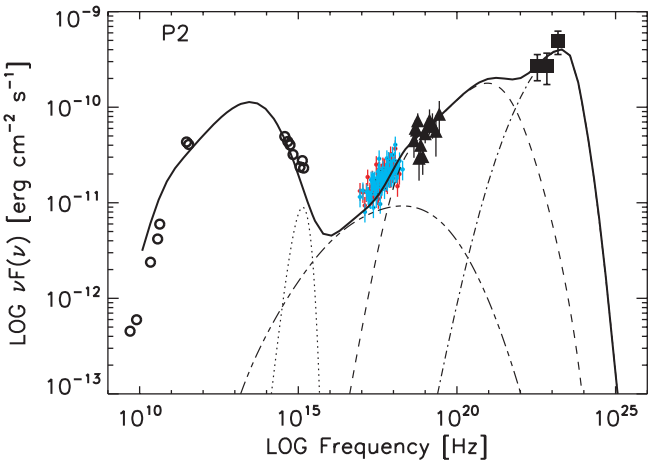

Figure 13. SED for the period P2, MJD 54,423.5–54,426.5 (see Figure 10). Filled squares represent the *AGILE* GRID data in the energy range 100–1000 MeV; filled triangles represent *INTEGRAL*/IBIS data in the energy range 20–200 keV (orbits 623+624); small filled circles represent *Swift*/XRT data in the energy range 0.3–10 keV (segments 003, 004, and 005); open symbols represent radio-to-UV data taken from Raiteri et al. (2008a), corresponding to MJD 54425. The dotted, dashed, dot–dashed, and triple-dot–dashed lines represent the accretion disk blackbody, the external Compton on the disk radiation, the external Compton on the BLR and SSC radiation, respectively.

(A color version of this figure is available in the online journal.)

GRID data in the energy range 100–1000 MeV; filled triangles represent *INTEGRAL*/IBIS data in the energy range 17–150 keV (orbits 623+624); small filled circles represent *Swift*/XRT data in the energy range 0.3–10 keV (segments 003, 004, and 005); open symbols represent radio-to-UV data taken from Raiteri et al. (2008a), corresponding to MJD 54,425.

A brief discussion of the modeling of both SEDs is presented in Section 8.

8. DISCUSSION

The long-term γ-ray activity of 3C 454.3 is one of the most interesting discoveries achieved by *AGILE* during its first six months of observations. The source was already detected in high state in 2007 July during a one-week *AGILE* ToO triggered by an intense optical flare detected by the WEBT. During that period, the source reached its highest intensity level, with an average γ-ray flux of $F_{E>100\,\mathrm{MeV}} = (280 \pm 40) \times 10^{-8}$ photons cm^{-2} s^{-1}. In 2007 November, 3C 454.3 showed prominent and prolonged γ-ray activity, with flaring episodes on a timescale of a few days and an average γ-ray flux of $F_{E>100\,\mathrm{MeV}} = (170 \pm 13) \times 10^{-8}$ photons cm^{-2} s^{-1}. This renewed activity triggered observations at different frequencies, allowing us to obtain an almost *simultaneous* SED coverage on 14 decades in energies. We dubbed 3C 454.3 as *crazy diamond* because of its dramatic variability at high energies revealed during the first half of the *AGILE* Observing Cycle-1. It has become clear that this source is playing the same role for *AGILE* as 3C 279 had for EGRET. The 3C 454.3 strong variability has also a clear signature at lower frequencies. As reported in Raiteri et al. (2008a), during the *AGILE* observation, on MJD 54,425 the source showed an extremely variable behavior in the *R* band, with a brightening of 0.33 mag in 2.3 h. In the same paper, the authors report other episodes of fast variability with flux variations of several tenths of mag in a few hours. Moreover, while in 2007 July 3C 454.3 exhibited its most intense optical flare there was a very moderate degree of γ-ray flux variability on a day-by-day timescale during the 2007 November campaign (see Figure 3), and we note a significant γ-ray flux variability on short timescales with at least two distinct flaring episodes (P1 and P2). It is interesting to note that in the optical band, 3C 454.3 also seems to display more rapid flares during the fall/winter 2007 WEBT campaign than those that occurred during the 2007 July monitoring (Raiteri et al. 2008b).

We compared the spectral properties of higher state periods, P1 and P2, with two lower state periods, P_low1 and P_low2, chosen to be of the same duration as P1 and P2 and corresponding to MJD 54,414.5–54,417.7 and MJD 54,420.5–54,423.5, respectively. Figure 14 shows the *AGILE* GRID spectra for periods P1 (red square), P2 (green star), P1_low1 (black circle), and P2_low2 (blue upside-down triangle). The 2007 July spectrum is also shown (cyan upside-down triangle). Although the statistics accumulated in only four days do not allow us to obtain a robust fit of the data, Figure 14 shows no clear spectral differences among different source intensity levels.

The correlation between the flux level and the spectral slope was extensively studied by means of the analysis of the EGRET data. Recently, Nandikotkur et al. (2007) have shown that there is no homogeneous behavior among EGRET blazars. Although they consider *long-term* spectral dependence on flux rather than *short-term* as in our case, our findings are in agreement with their results on 3C 454.3. Figure 3 in Nandikotkur et al. (2007) shows no spectral variation despite a flux variation of about a factor of 4.

Different emission mechanisms can be invoked to explain the γ-ray emission and the different spectral states. In the leptonic scenario, the low-frequency peak is interpreted as synchrotron radiation from high-energy electrons in the relativistic jet, while the high-energy peak can be produced by IC on different *flavors* of seed photons. In the synchrotron self-Compton (SSC) model (Ghisellini et al. 1985; Bloom & Marscher 1996), the seed photons come from the jet itself. Alternatively, the seed photons can be those of the accretion disk (external Compton scattering of direct disk radiation, ECD, Dermer et al. (1992)), or those of the broad-line region (BLR) clouds (external Compton scattering from clouds, ECC, Sikora et al. (1994)). The target

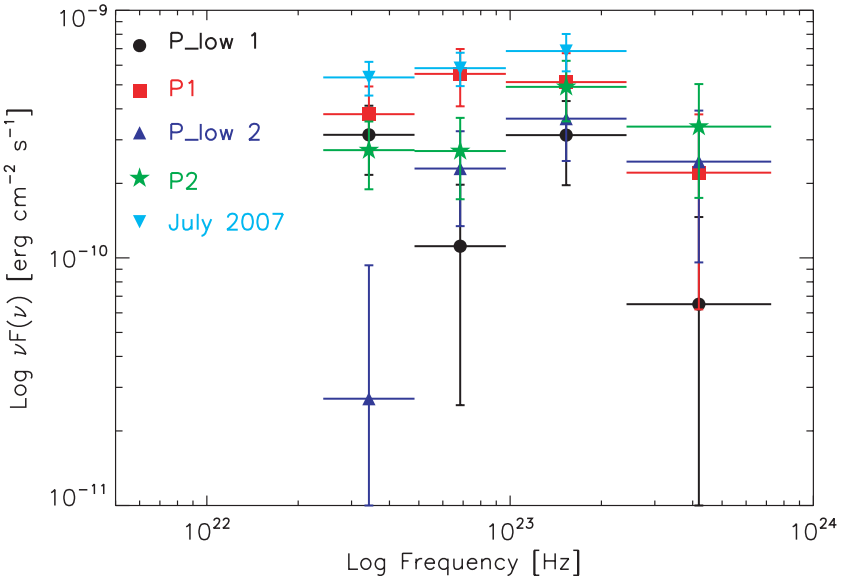

Figure 14. *AGILE* GRID spectra for periods P1 (red squares), P2 (green stars), P1_low1 (black circles), P2_low2 (blue upside-down triangles). The 2007 July spectrum is also shown (cyan upside-down triangles).

(A color version of this figure is available in the online journal.)

seed photons can also be those produced by the infrared (IR) dust torus surrounding the nucleus (external Compton scattering from IR dust, ERC(IR), Sikora et al. (2002)).

Błażejowski et al. (2000) showed that the ERC(IR) emission peak is at lower frequencies (soft γ-ray), more suitable for MeV blazars, while our SEDs show a peak for the EC component in the GeV region of the spectrum. The average photon index during this 2007 November campaign ($\Gamma_{AGILE} = 1.73 \pm 0.16$) is harder than the time-averaged one reported in Nandikotkur et al. (2007) ($\Gamma_{\rm EGRET} = 2.22 \pm 0.06$) for EGRET. During intense γ-ray flares, the ECC and ECD processes play a major role, and the softness or the hardness of the resulting spectrum is controlled by the dominant component, as illustrated in Hartman et al. (2001) for 3C 279. In the case of 3C 454.3, the ECC component seems to play a major role, as we will show from the SED modeling.

We fit the SEDs for the P1 and P2 gamma-ray flaring episodes by means of a one-zone leptonic model, considering the contributions from SSC and from external seed photons originating both from the accretion disk and from the BLR. The emission along the jet is assumed to be produced in a spherical blob with comoving radius R by accelerated electrons characterized by a comoving broken power-law energy density distribution of the form

$$n_e(\gamma) = \frac{K\gamma_{\rm b}^{-1}}{(\gamma/\gamma_{\rm b})^{\alpha_{\rm l}} + (\gamma/\gamma_{\rm b})^{\alpha_{\rm h}}}, \quad (2)$$

where γ is the electron Lorentz factor assumed to vary between $10 < \gamma < 1.5 \times 10^4$, $\alpha_{\rm l}$ and $\alpha_{\rm h}$ are the pre- and postbreak electron distribution spectral indices, respectively, and $\gamma_{\rm b}$ is the break energy Lorentz factor. We assume that the blob contains a random average magnetic field B and that it moves with a bulk Lorentz factor Γ at an angle Θ_0 with respect to the line of sight. The relativistic Doppler factor is then $\delta = [\Gamma(1 - \beta\cos\Theta_0)]^{-1}$, where β is the usual blob bulk speed in units of the speed of light.

Our modeling of the 3C 454.3 high-energy emission is based on an IC model with two main sources of external target photons: (1) an accretion disk characterized by a blackbody spectrum peaking in the UV with a bolometric luminosity L_d for an IC-scattering blob at a distance L from the central part of the disk; (2) a BLR with a spectrum peaking in the V band and assumed to reprocess 10% of the irradiating continuum (Tavecchio & Ghisellini 2008; Raiteri et al. 2007, 2008b).

These two regions contribute to the ECD and the ECC, respectively, and it is interesting to test the relative importance of the two components that can be emitted by the relativistic jet of 3C 454.3 under different conditions. A complete theoretical analysis of the model, and of the interplay among the different parameters is beyond the scope of this paper and will be presented in a forthcoming paper. We summarize here the main results of our best model characterized by an interesting set of physical parameters.

Table 3 shows the best-fit parameter of our modeling of the flaring-state SEDs corresponding to the P1 and P2 phases of Figure 10. Our best-fit parameter values are: $B \sim 10$ G, $\Gamma = 8.4$, $\Theta_0 = 2.6^\circ$, and $r = 0.05$ pc, where r is the distance between the accretion disk and the emitting region. In both Figures 12 and 13, the dotted, dashed, dot–dashed, and triple-dot–dashed lines represent the contributions of the accretion disk blackbody, the external Compton on the disk radiation, the external Compton on the BLR, and SSC radiation, respectively.

We note that during both the P1 and P2 episodes, the ECD contribution can account for the soft and hard X-ray portions of the spectrum, which show a moderate, if any, time variability. However, we note that the ECD component alone cannot account for the hardness of the γ-ray spectrum. We therefore argue that in the *AGILE* energy band, a dominant contribution from ECC seems to provide a better fit of the data during the γ-ray flaring states P1 and P2. Moreover, Table 3 shows that the data of both SEDs can be fitted by very similar model parameters. We note, however, that the high-energy part of the electron energy distribution appears to be softer during the P2 episode as compared to the electron distribution of the P1 flare. Hartman et al. (2001) find, for 3C 279, a relevant contribution of the SSC component in the X-ray–soft γ-ray bands. However, their average values for γ_1 and γ_2 are much higher (a factor of 5–10)

Table 3
Input Parameters for the Model of P1 and P2 SEDs. See text for details.

Parameter	SED P1	SED P2	Units
α_l	2.1	2.2	
α_h	4.5	5.0	
γ_{min}	10	10	
γ_b	500	500	
K	14	12	cm^{-3}
R	35	35	10^{15} cm
B	10	8	G
δ	14.64	14.64	
L_d	5	5	10^{46} erg s^{-1}
r	0.05	0.05	pc
Θ_0	2.6	2.6	deg
Γ	8.4	8.4	

than ours, resulting in an increase of the ratio SSC/Sync $\propto \gamma^2$. Thus, for the Hartman et al. (2001) choice of parameters, the SSC contribution becomes relevant at higher frequencies and of the same order as the ECD contribution.

Our results can be compared with those obtained by Jorstad et al. (2005). By means of total and polarized images obtained at the Very Long Baseline Array (VLBA) at 7 mm, they were able to compute the global parameters of the source jet, estimating $\langle\Gamma\rangle = 15.6 \pm 2.2$, $\langle\delta\rangle = 24.6 \pm 4.5$, $\theta = (0.8 \pm 0.2)^\circ$, and $\langle\Theta_0\rangle = (1.3 \pm 1.2)^\circ$, where $\langle\Gamma\rangle$ and $\langle\delta\rangle$ are the average Lorentz and Doppler factors, respectively, while θ and $\langle\Theta_0\rangle$ are the intrinsic half-opening angle of the jet and the angle between the jet axis and the line of sight, respectively. We note, however, that the jet parameters derived so far were obtained by means of data collected in earlier epochs with respect to our observations, and refer to average values of different jet components.

The energetics of 3C 454.3 can be computed by estimating the isotropic luminosity in the γ-ray band, L_γ^{iso}, and comparing it with the Eddington, the bolometric, and the particle injection luminosities. For a given source with redshift z, the isotropic-emitted luminosity in the energy band ϵ is defined as

$$L(z)_\epsilon = \frac{4\pi F d_l^2(z)}{(1+z)^{(1-\alpha)}}, \quad (3)$$

where, in our case, ϵ is the γ-ray energy band with $E_{min} = 100$ MeV and $E_{max} = 10$ GeV, α is the γ-ray energy spectral index, $F(\nu) \propto \nu^{-\alpha}$ is the energy differential flux, $F = \int_{E_{min}/h}^{E_{max}/h} F(\nu)\, d\nu$ is the flux in the γ-ray band, and the luminosity distance is given by

$$d_l(z_1, z_2) = (1+z_2)^2 \times \frac{c/H_0}{1+z_2} \int_{z_1}^{z_2} [E(z)]^{-1} dz, \quad (4)$$

where $z_1 = 0$, $z_2 = z_{src}$ and

$$E(z) = \sqrt{\Omega_M (1+z)^3 + (1 - \Omega_M - \Omega_\Lambda)(1+z)^2 + \Omega_\Lambda}, \quad (5)$$

where H_0 is the Hubble constant, Ω_M and Ω_Λ are the contributions of the matter and of the cosmological constant, respectively, to the density parameter. Hereafter, we assume $H_0 = 70$ km s^{-1} Mpc^{-1}, $\Omega_M = 0.3$, and $\Omega_\Lambda = 0.7$. Using the observed average γ-ray flux, we obtain $L_\gamma^{iso} = 3.9 \times 10^{48}$ erg s^{-1}.

Moreover, from the values quoted in Table 3 and from Equation (2) we can compute the particle injection luminosity, L_{inj}, obtaining

$$L_{inj} = \pi\, R^2\, \Gamma^2\, c \int [d\gamma\; m_e\, c^2 \gamma\, n(\gamma)] = 3 \times 10^{44} \text{ erg s}^{-1}. \quad (6)$$

Assuming for 3C 454.3 a black hole mass $M_{BH} = 4.4 \times 10^9\ M_\odot$ (Gu et al. 2001), we obtain an Eddington luminosity of the order of $L_{Edd} = 5.7 \times 10^{47}$ erg s^{-1} to be compared with the bolometric luminosity $L_{bol} = 1.9 \times 10^{47}$ erg s^{-1} reported in Woo & Urry (2002).

We obtain, therefore, that the source energetic is comparable to the value obtained by Tavecchio et al. (2007) for the power of the inner portion of jet, a few $\times 10^{47}$ erg s^{-1}.

9. CONCLUSIONS

The *AGILE* mission is particularly suited to monitor a large number of potential γ-ray sources. The *AGILE* pointings during 2007 November, despite being centered approximately in the Cygnus region of the Galactic plane, revealed the very prominent γ-ray activity of the blazar 3C 454.3. The *AGILE* detection of this blazar prompted a series of important multiwavelength observations. The electromagnetic emission of 3C 454.3 could be determined with an unprecedented coverage over 14 orders of magnitude in energy during a period that included a substantial fraction of the months of 2007 November and December. Results of the *AGILE* data and related multifrequency campaign carried out in 2007 December will be presented in a forthcoming paper.

We reported in this paper the main results of our *AGILE* and associated multifrequency campaigns during 2007 November. Our results can be summarized as follows.

1. The γ-ray emission from 3C 454.3 dominated the whole extragalactic sky as monitored by *AGILE* during its first year of scientific operations.
2. Our γ-ray data show remarkable variability on a daily timescale for an FSRQ.
3. Emission in the optical range appears to be correlated with that at γ-ray energies above 100 MeV.
4. Variability in the soft and hard X-ray range is less sensitive to the short-timescale variations of the optical flux.
5. The average γ-ray spectrum during the whole campaign is substantially harder than that reported in previous observations.
6. We determined the SEDs for episodes of relatively high γ-ray emission.
7. Our results support the idea that the dominant emission mechanism in γ-ray energy band is the IC scattering of external photons from the BLR clouds scattering off the relativistic electrons in the jet.

We thank the referee for his/her very prompt and constructive comments. The *AGILE* Mission is funded by the Italian Space Agency (ASI) with scientific and programmatic participation by the Italian Institute of Astrophysics (INAF) and the Italian Institute of Nuclear Physics (INFN). This investigation was carried out with partial support under ASI contract I/089/06/1. This work is partly based on data taken and assembled by the WEBT collaboration and stored in the WEBT archive at the Osservatorio Astronomico di Torino–INAF (http://www.to.astro.it/blazars/webt/). We thank the *Swift* and *INTEGRAL* teams for making these observations

possible, particularly the duty scientists and science planners. M.T.F., A.B., and P.U. acknowledge ASI/INAF contract 023/05/0.

Facilities: AGILE, *Swift*, *INTEGRAL*, WEBT, REM

REFERENCES

Aller, M. F., et al. 1997, in AIP Conf. Ser. 410, Proc. Fourth Compton Symposium, ed. C. D. Dermer, M. S. Strickman, & J. D. Kurfess (Melville, NY: AIP), 1423
Barthelmy, S. D., et al. 2005, Space Sci. Rev., 120, 143
Błazejowski, M., Sikora, M., Moderski, R., & Madejski, G. M. 2000, ApJ, 545, 107
Bloom, S. D., & Marscher, A. P. 1996, ApJ, 461, 657
Burrows, D. N., et al. 2005, Space Sci. Rev., 120, 165
Celotti, A., & Ghisellini, G. 2008, MNRAS, 385, 283
Chen, A., et al. 2007, Astron. Telegram, 1278, 1
Conconi, P., et al. 2004, in Proc. SPIE 5492, Ground-Based Instrumentation for Astronomy, ed. A. F. M. Moorwood, & M. Iye (Bellingham, WA: SPIE), 1602
Dermer, C. D., Schlickeiser, R., & Mastichiadis, A. 1992, A&A, 256, L27
Edelson, R. A., & Krolik, J. H. 1988, ApJ, 333, 646
Feroci, M., et al. 2007, Nucl. Instrum. Methods Phys. Res. A, 581, 728
Fiorucci, M., Tosti, G., & Rizzi, N. 1998, PASP, 110, 105
Fuhrmann, L., et al. 2006, A&A, 445, L1
Gehrels, N., et al. 2004, ApJ, 611, 1005
Ghisellini, G., Foschini, L., Tavecchio, F., & Pian, E. 2007, MNRAS, 382, L82
Ghisellini, G., Maraschi, L., & Treves, A. 1985, A&A, 146, 204
Giommi, P., et al. 2006, A&A, 456, 911
Giuliani, A., Chen, A., Mereghetti, S., Pellizzoni, A., Tavani, M., & Vercellone, S. 2004, Mem. SAIt Suppl., 5, 135
González-Pérez, J. N., Kidger, M. R., & Martín-Luis, F. 2001, AJ, 122, 2055
Gu, M., Cao, X., & Jiang, D. R. 2001, MNRAS, 327, 1111
Hartman, R. C., et al. 1992, IAU Circ., 5477, 2
Hartman, R. C., et al. 1993, ApJ, 407, L41
Hartman, R. C., et al. 1999, ApJS, 123, 79
Hartman, R. C., et al. 2001, ApJ, 553, 683
Hufnagel, B. R., & Bregman, J. N. 1992, ApJ, 386, 473
Jorstad, S. G., et al. 2005, AJ, 130, 1418
Kalberla, P. M. W., Burton, W. B., Hartmann, D., Arnal, E. M., Bajaja, E., Morras, R., & Pöppel, W. G. L. 2005, A&A, 440, 775
Labanti, C., et al. 2006, in Proc. SPIE, 6266, 62663Q
Mattox, J. R., et al. 1993, ApJ, 410, 609
McLaughlin, M. A., Mattox, J. R., Cordes, J. M., & Thompson, D. J. 1996, ApJ, 473, 763
Mücke, A., & Protheroe, R. J. 2001, Astropart. Phys., 15, 121
Mücke, A., Protheroe, R. J., Engel, R., Rachen, J. P., & Stanev, T. 2003, Astropart. Phys., 18, 593
Nandikotkur, G., Jahoda, K. M., Hartman, R. C., Mukherjee, R., Sreekumar, P., Böttcher, M., Sambruna, R. M., & Swank, J. H. 2007, ApJ, 657, 706
Perotti, F., Fiorini, M., Incorvaia, S., Mattaini, E., & Sant'Ambrogio, E. 2006, Nucl. Instrum. Methods Phys. Res. A, 556, 228
Peterson, B. M. 2001, in Advanced Lectures on the Starburst–AGN Connection, ed. I. Aretxaga, D. Kunth, & R. Mújica (Singapore: World Scientific), 3
Pian, E., et al. 2006, A&A, 449, L21
Prest, M., Barbiellini, G., Bordignon, G., Fedel, G., Liello, F., Longo, F., Pontoni, C., & Vallazza, E. 2003, Nucl. Instrum. Methods Phys. Res. A, 501, 280
Pucella, G., et al. 2007, Astron. Telegram, 1300, 1
Raiteri, C. M., Villata, M., Lanteri, L., Cavallone, M., & Sobrito, G. 1998, A&AS, 130, 495
Raiteri, C. M., et al. 2008a, A&A, 485, L17
Raiteri, C. M., et al. 2008b, A&A, in press (arXiv:0810.2424)
Raiteri, C. M., et al. 2007, A&A, 473, 819
Roming, P. W. A., et al. 2005, Space Sci. Rev., 120, 95
Senziani, F., Novara, G., de Luca, A., Caraveo, P. A., Belloni, T., & Bignami, G. F. 2007, A&A, 476, 1297
Sikora, M., Begelman, M. C., & Rees, M. J. 1994, ApJ, 421, 153
Sikora, M., Błazejowski, M., Moderski, R., & Madejski, G. M. 2002, ApJ, 577, 78
Tavani, M., et al. 2008a, Nucl. Instrum. Methods Phys. Res. A, 588, 52
Tavani, M., et al. 2008b, A&A, submitted (arXiv:0807.4254v1)
Tavecchio, F., & Ghisellini, G. 2008, MNRAS, 386, 945
Tavecchio, F., Maraschi, L., Wolter, A., Cheung, C. C., Sambruna, R. M., & Urry, C. M. 2007, ApJ, 662, 900
Torres, D. F., Romero, G. E., Combi, J. A., Benaglia, P., Andernach, H., & Punsly, B. 2001, A&A, 370, 468
Tosti, G., et al. 2004, in Proc. SPIE 5492, Ground-Based Instrumentation for Astronomy, ed. A. F. M. Moorwood, & M. Iye (Bellingham, WA: SPIE), 689
Ubertini, P., et al. 2003, A&A, 411, L131
Vercellone, S., et al. 2007, Astron. Telegram, 1160, 1
Vercellone, S., et al. 2008, ApJ, 676, L13
Villata, M., et al. 2004, A&A, 424, 497
Villata, M., et al. 2006, A&A, 453, 817
Villata, M., et al. 2007, A&A, 464, L5
Woo, J.-H., & Urry, C. M. 2002, ApJ, 579, 530
Zerbi, F. M., et al. 2004, in Proc. SPIE 5492, Ground-Based Instrumentation for Astronomy, ed. A. F. M. Moorwood, & M. Iye (Bellingham, WA: SPIE), 1590